THE JOURNAL OF PHYSICAL CHEMISTRY C

Article

pubs.acs.org/JPCC

Role of Carbon Nanotubes in Dye-Sensitized TiO_2-Based Solar Cells

Jiazang Chen,*,† Bo Li, Jianfeng Zheng, Jianghong Zhao, and Zhenping Zhu*

State Key Laboratory of Coal Conversion, Institute of Coal Chemistry, Chinese Academy of Sciences, Taiyuan 030001, China

Supporting Information

ABSTRACT: Incorporation of low-dimensional carbon nanostructures such as carbon nanotubes (CNTs) and graphene sheets into the semiconductor electrodes is a common approach to improve the charge collection and photovoltaic performance of dye-sensitized solar cells. In this work, we clarify the role of CNTs in the semiconductor electrodes by investigating and comparing the electronic process in the dye-sensitized TiO_2-based photovoltaic devices. The results show that the formed CNT−TiO_2 Schottky junction plays a crucial role in the photovoltaic characteristics. According to the thermionic emission theory, the variation of the photocurrent over the voltage of the cells strongly depends on the height of the Schottky barrier. When the output voltage is low, the intrinsic one-dimensional carbon nanostructures can facilitate electron transport. With the voltage of the cell increasing, the energy dissipation on the Schottky junction increases dramatically and CNTs gradually lose the role of electron transport channels. At the high voltage range, however, leakage of electrons via the CNTs becomes predominant. By virtue of the charge transport channels of CNTs, increments of 44% in photocurrent at short-circuit condition and 18.7% in the overall energy conversion are achieved. Our results provide a basic understanding of the role of CNTs in solar energy conversion.

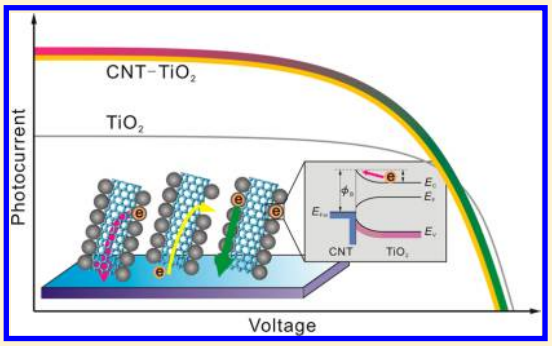

1. INTRODUCTION

In dye-sensitized solar cells (DSSCs),[1−3] the competition between the transport of electrons through the porous semiconductor and the recombination of electrons with I_3^- ions on the semiconductor−electrolyte interface determines the electron collection efficiency and overall energy conversion efficiency.[4−8] Therefore, promotion of transport of photogenerated electrons in the semiconductor electrode becomes one of the most promising ways to improve the photovoltaic performance of the cells. Thus far, many approaches, including formation of one/zero-dimensional homogeneous nanosctructured architecture,[9−12] modulation of the intraband electronic states of the semiconductor,[13−15] and incorporation of heterogeneous conducting nanostructures (carbon nanostructures such as carbon nanotubes, graphene sheets are most common) as special *charge transport channels* into the semiconductor electrodes,[16−35] have been proposed. Among them, formation of composite electrodes by incorporation of conducting materials into the mesoporous electrodes is much easier to be carried out, and results on the beneficial effects of the carbon nanostructures on the energy conversion of DSSCs have been widely reported.[16−35]

Carbon nanostructures are extensively used as additives in composite electrode to promote electric and thermal conductivity, reinforce the mechanical strength, and enhance the flexibility. Similarly, introduction of these materials into the semiconductor electrodes can also reduce the resistance of the host materials. Take carbon nanotubes (CNTs) as an example: incorporation of CNTs into semiconductor electrodes has been carried out by several groups.[16,17,20−23] Mainly, the purpose for introduction of CNTs into the mesoporous electrodes is that CNTs would fill the role of the special channels to facilitate electron transport and reduce the resistance of the electrodes, as illustrated in Figure 1.[17−19,24−26] In this assumption it is

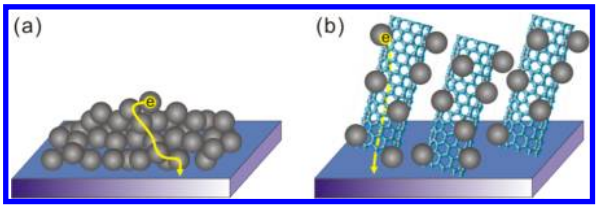

Figure 1. Schematic diagrams for the photogenerated electron transport route in blank semiconductor electrodes (a) and carbon nanotube-incorporated electrodes (b) of dye-sensitized solar cells.

believed that during the transport of electrons through mesoporous films the photogenerated electrons can directly transfer to the transparent conducting oxide (TCO) substrate via the CNTs without encountering the numerous grain boundaries. Thus, the transmission line model describes that the electronic process for common photovoltaic cells[36−39] should be modified correspondingly when the function of CNTs is taken into account (Figure 2). For the composite electrode, the charge transport resistance, R_t, would be ideally the numerous individual charge transfer resistance of the

Received: May 18, 2012
Revised: June 18, 2012
Published: June 21, 2012

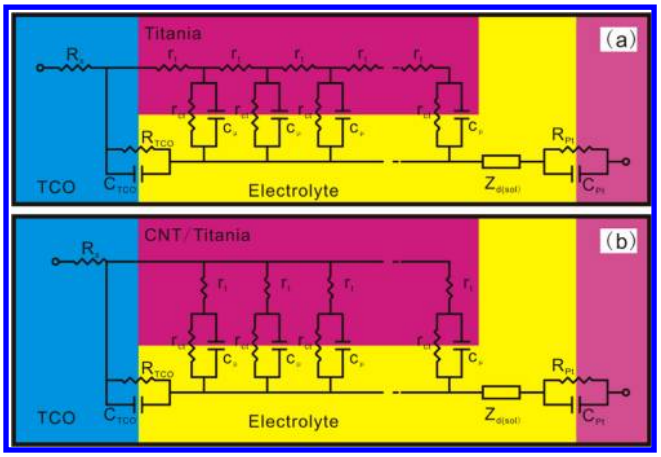

Figure 2. Schemes for the transmission line of dye-sensitized solar cells without (a) and with (b) incorporation of carbon nanotubes into the semiconductor electrodes.[36−39]

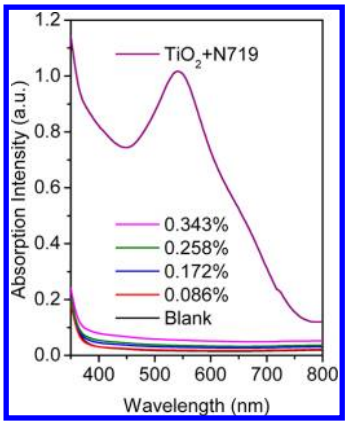

Figure 3. UV−vis absorption spectra for the CNTs-incorporated TiO_2 electrodes and dye-sensitized TiO_2 electrode (without CNTs).

CNT−TiO_2, $r_{t,Ti-CNT}$ connected in parallel: $R_t = r_{t,Ti-CNT}/n$ (Figure 2b) rather than the sum of the interparticle resistance, $r_{t,Ti-Ti}$ connected in series: $R_t = r_{t,Ti-Ti} \times n$ for a common electrode (Figure 2a). On the other hand, the charge recombination resistance on the semiconductor−electrolyte interface, R_{ct}, representing the numerous charge transfer resistances between individual particle and electrolyte connected in parallel, $R_{ct} = r_{ct}/n$, is identical for cells with and without CNTs (Figure 2). According to the expression $\eta_{CC} = 1 - R_t/R_{ct}$,[13] the charge collection efficiency (η_{CC}) for the composite electrode-based cells would no longer be influenced by the number of interparticle boundaries that the electrons encountered as they transport through the common semiconductor films.

Although CNTs would bring many benefits to the transport of electrons as described above, improvement in photovoltaic performance of the DSSCs can only be realized at a very narrow concentration range of CNTs in the semiconductor electrodes (commonly less than 0.5 wt %).[16−21] When the CNT concentration exceeds the optimized value, the photocurrent and energy conversion efficiency of the cells decrease rapidly. Therefore, it is of great importance to elucidate the strange phenomenon and clarify the role of CNTs in the semiconductor electrodes to get better performance. The issue, competition between light harvesting by dye molecules and photon loss by CNTs, has been widely proposed to explain the phenomena.[40] However, it is somewhat intuitive and not able to give satisfied elucidation. Intrinsically, carbon materials can absorb the photons from a very wide spectrum, while in the composite electrode the amount of CNTs is very small and almost all of them were coated by semiconductor nanoparticles (Figure 3). After sensitization of the nanoparticles by the high absorbance dye, there is almost "no chance" for the photons to access the CNTs. On the other hand, a small fluctuation of CNT concentration in the semiconductor electrodes would not cause severe loss of photon proportion for the dye molecules. The very sensitive effect of the CNT concentration in the semiconductor electrodes should be attributed to other issues, i.e., the electronic process in the porous electrodes, especially electron transport through the CNT−semiconductor junction. In this work, leakage of electrons via the naked CNTs and the effect of the Schottky barrier height on charge transport through the CNT−TiO_2 junction have been investigated and proposed to explain the influence of CNTs on the photovoltaic characteristics of the CNTs-incorporated TiO_2 electrode-based DSSCs.

2. EXPERIMENTAL SECTION

2.1. Preparation of TiO_2 Nanoparticles. TiO_2 nanoparticles were prepared according to our previously reported procedure by hydrothermal synthesis starting from titanium(IV) *n*-butoxide.[41] Briefly, 40 mL of titanium(IV) butoxide was dropwisely added into 240 mL of 0.1 M HNO_3 under vigorous stirring. Then, the obtained slurry was rapidly heated to 80 °C and kept for 8 h. After peptization, the colloidal solution was moved to a self-sealed Teflon-lined autoclave that was heated for 12 h at 230 °C to grow TiO_2 nanoparticles. After reaction, a desired amount of CNT−water dispersion (0.1 mg/mL) was added dropwise into the hydrothermal product. In order to achieve a good interaction with the TiO_2 nanoparticles, the CNTs were first functionalized prior to use.[42] Briefly, 1 g of multiwalled carbon nanotubes (~40 nm in diameter) was mixed with 50 mL of HNO_3 (14 M) and refluxed at 80 °C for 8 h. Then the CNTs were filtered out, washed with water, and dried at 60 °C overnight under vacuum. Afterward, carboxylic groups were introduced in the functionalized product (Figure S1, Supporting Information). The CNT−water dispersion was obtained by dispersing the HNO_3-treated carbon nanotubes into water under sonication.

2.2. Fabrication of DSSCs. The mixed dispersion was then concentrated in a rotary evaporator and evaporated at 40 °C to a final TiO_2 concentration of ~15 wt %. The as-prepared pastes were deposited by doctor-blade technique onto fluorine-doped tin oxide conducting glass (FTO, 14 ohm per square, Nippon Glass Sheet) by preparing an active area of 0.50 cm^2. Seven pastes, with carbon nanotube concentrations of 0, 0.021, 0.043, 0.086, 0.172, 0.258, and 0.343 wt %, were used to prepare TiO_2 photoelectrodes. The thickness of the films was controlled by adjusting the thickness of adhesive tapes (here the thickness of the TiO_2 films after calcination were about 12 μm). The film was then heated to 400 °C at a rate of 15 °C/min and kept at 400 °C for 30 min. After cooling to 80 °C, the TiO_2 electrode was immersed overnight in a solution of ruthenium dye solution (*cis*-di(thiocyanato)-*N*,*N*′-bis(2,2′-bipyridyl-4-carboxyl acid-4′-tetrabutylammonium carboxylate)ruthenium(II) (also known as N-719) that was dissolved in acetonitrile with a concentration of 0.5 mM). The electrode was then rinsed with acetonitrile and dried. Then one drop of iodine-containing

electrolyte was deposited onto the surface of the electrode and penetrated inside the TiO_2 film via capillary action. The electrolyte was composed of 0.1 M of lithium iodide (LiI), 0.6 M of tetrabutylammonium iodide (TBAI), 0.05 M of iodine (I_2), and 0.5 M of 4-*tert*-butylpyridine that was dissolved in acetonitrile. A platinized FTO counter electrode was then clipped onto the top of TiO_2 photoelectrode to form a photovoltaic device.

2.3. Photoelectrochemistry and Electrochemistry. The photovoltaic properties of the DSSCs were characterized by recording the photocurrent−voltage (J−V) curves under illumination of A.M. 1.5 G (100 mW/cm^2). Illumination was provided by performing a San-Ei solar simulator. The effect of carbon nanotubes on the electronic process was characterized by intensity-modulated photocurrent/photovoltage spectroscopy (IMPS/IMVS) measurements, which were carried out on a computer-controlled Zahner Im6ex CIMPS potentiostat. Electrochemical impedance measurements of the cells were performed with a Zahner Im6ex potentiostat with a frequency of 0.005−500k Hz; the amplitude of the ac signal is 10 mV. The obtained impedance spectra were fitted with Z-view software.

3. RESULTS AND DISCUSSION

3.1. Effects of Carbon Nanotubes on the Photovoltaic Characteristics of the Cells. *3.1.1. Charge Transport in Semiconductor Electrodes.* Electron transport in DSSCs is driven mainly by diffusion due to the effective electrolyte shielding of space charge.[43] According to the classical multiple trapping (MT) framework,[44,45] the effective diffusion coefficient for a cell is given by

$$D_n = \left(\frac{\partial n_c}{\partial n_t}\right) D_0 \tag{1}$$

where D_0 is the diffusion coefficient of the electron at the energy level of the low edge of the conduction band, n_t is the trapped electron density, and n_c is the conduction band electron density. Under quasi-steady state, the effective diffusion coefficient of the electron in a TiO_2 electrode can be obtained using small perturbation techniques such as IMPS and impedance spectroscopy. Here we calculate D_n from the electron transport time with the equation[46]

$$D_n = \frac{L_d^2}{2.35 \times \tau_d} \tag{2}$$

where τ_d is the electron transport time constant and L_d is the thickness of the semiconductor films. The electron transport time constant can be evaluated from the expression $\tau_d = 1/(2\pi f_{IMPS})$, in which f_{IMPS} is the characteristic frequency derived from the IMPS measurements, i.e., the frequency of the lowest imaginary component of the IMPS pattern.[47,48]

Figure 4 illustrates the influence of CNT concentration in the TiO_2-based electrodes on the electron transport time constants and electron diffusion coefficients. It can be seen that the time constant decreases as the CNT concentration increases, suggesting transport of electrons in the CNTs-incorporated electrode is much faster. By substituting the time constant into eq 2 it can be seen that the electron diffusion coefficients increase with the CNT concentration, indicating that introduction of highly conductive carbon nanostructures would be favorable to charge transport in the composite electrodes.

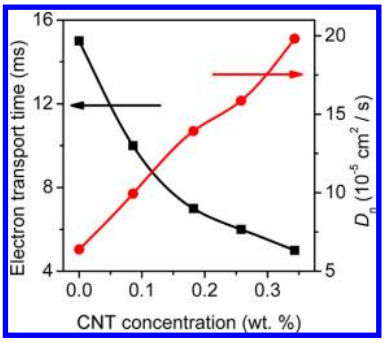

Figure 4. Characteristic time constants for transport of photogenerated electrons (black square) and corresponding charge diffusion coefficient (red cycle) in the electrodes with various concentrations of carbon nanotubes.

3.1.2. Photovoltaic Performance. Figure 5 presents the effects of CNT concentration on the photovoltaic characteristics of the cells. In order to directly demonstrate the impact of CNTs, the photovoltaic parameters including open-circuit voltage (V_{OC}), short-circuit photocurrent density (J_{SC}), fill factor (FF), and overall energy conversion efficiency (η) were normalized to the related value of the blank cell (Figure 6). It can be seen that J_{SC} plays a predominant role on the variation

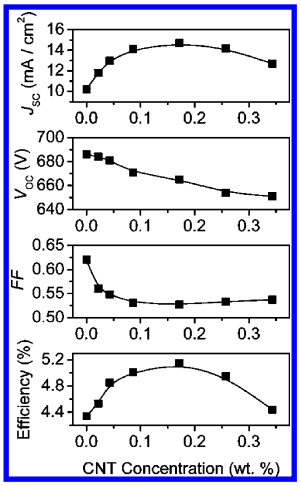

Figure 5. Photovoltaic characteristic parameters for the cells with various concentrations of carbon nanotubes in the semiconductor electrodes.

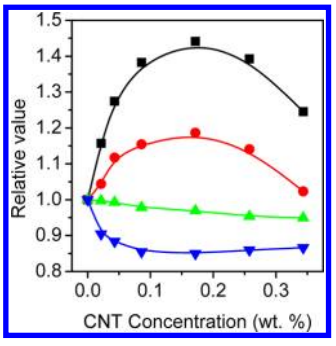

Figure 6. Significance of CNT concentration on the photovoltaic characteristics. J_{SC} (black square), η (red cycle), V_{OC} (green up triangle), and FF (blue down triangle) for CNT-containing cells are normalized to the related value of the blank one.

dx.doi.org/10.1021/jp304845t | J. Phys. Chem. C 2012, 116, 14848−14856

of the value of η, while FF and V_{OC} are only changed slightly through the whole CNT concentration range. This phenomenon matches with the primary purpose of introduction of CNTs into the porous semiconductor electrodes being to facilitate charge transport and charge collection.

In the low-concentration range (less than 0.172 wt %), the photocurrent as well as the energy conversion efficiency of the cells monotonously increase with the CNT concentration. For example, values of J_{SC} and η for the blank cell are 10.2 mA/cm^2 and 4.34%, respectively. By incorporation of CNTs into the TiO_2 films the J_{SC} value changed dramatically from 10.2 to 14.7 mA/cm^2 as the concentration of CNTs increases. By virtue of the photocurrent increment, the energy conversion efficiency of 5.15% was obtained when the concentration of CNTs in the semiconductor is 0.172 wt %. Compared with the cell based on blank TiO_2 electrode, an increment of ~18.7% is achieved. Further increase in the concentration of CNTs in the electrodes resulted in an undesirable decrease in photocurrent and energy conversion efficiency. The effects of CNTs on photovoltaic characteristics in our cells are very similar with literature-reported phenomena as well as that of graphene introduced into the porous semiconductor films.[18,22,24,25,49,50]

3.2. Charge Leakage via Carbon Nanotubes. *3.2.1. Electron Diffusion Length and Collection Efficiency.* Although CNTs can increase the electron diffusion coefficient and improve the photovoltaic performance of the cells to a certain extent, the photocurrent or energy conversion efficiency is not monotonously increased with the CNT concentration. Thus, it is of great importance to elucidate this phenomenon in the semiconductor electrodes and photovoltaic cells.

The electron diffusion length, L_n, and the closely related parameter electron collection efficiency, η_{cc}, are characteristic features which have a predominant influence on the photocurrent of the cells. The values of the electron diffusion length and electron collection efficiency can be obtained with the expressions

$$\eta_{CC} = 1 - \frac{\tau_d}{\tau_n} \tag{3a}$$

and

$$L_n = \sqrt{D_n \tau_n} \tag{3b}$$

where τ_n is the electron lifetime, which is a central quantity to determine the interfacial charge recombination dynamics in the cell and a strong function of the Fermi level or the open-circuit voltage, V_{OC}. Electron lifetime can be measured by small perturbation techniques at a fixed steady state such as IMVS, impedance spectroscopy, and transient technique, like open-circuit voltage decay.[51] Here, the electron lifetime was evaluated from IMVS patterns in terms of the expression

$$\tau_n = 1/(2\pi f_{IMVS})$$

Figure 7a shows the relationship between the electron lifetime, τ_n, and the CNT concentration. It is clear that the electron lifetime decreases with CNT concentration, suggesting that the CNTs will increase the rate of charge recombination. Thus, transport and recombination of the charge will partly offset each other as the CNTs are introduced into the semiconductor electrode. By substituting τ_n into eqs 3a and 3b, the value of η_{cc} and L_n can be obtained, as shown in Figure 7b. Similar to the situation of the photocurrent (Figures 5 and 6),

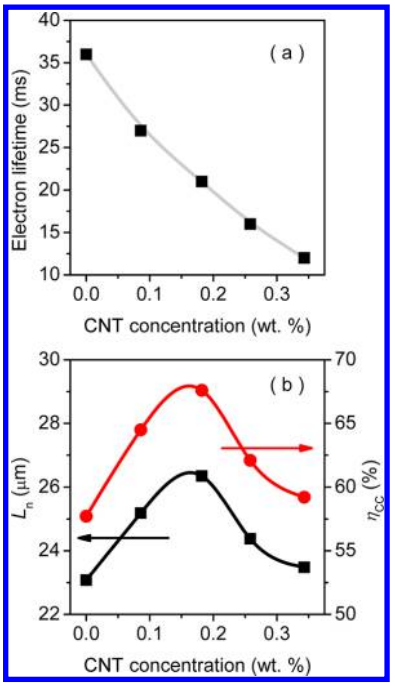

Figure 7. (a) Electron lifetime constants obtained from the intensity-modulated photovoltage spectroscopy patterns for cells with various concentrations of carbon nanotubes in the electrodes. (b) Electron diffusion length (black square) and electron collection efficiency (red cycle) for cells with various concentrations of carbon nanotubes in the semiconductor electrodes.

η_{cc} and L_n also exhibit optimized values at the position in which the CNT concentration is 0.172 wt %.

3.2.2. Charge Leakage. In order to gain further insight into charge collection, the feature of the interfacial charge recombination was investigated. Charge recombination on the interface of semiconductor−electrolyte can be described by the R_{ct} value, which can be obtained from impedance results. Figure 8a presents the typical electrochemical impedance spectroscopy (EIS) pattern obtained under illumination. The R_{ct} value for the

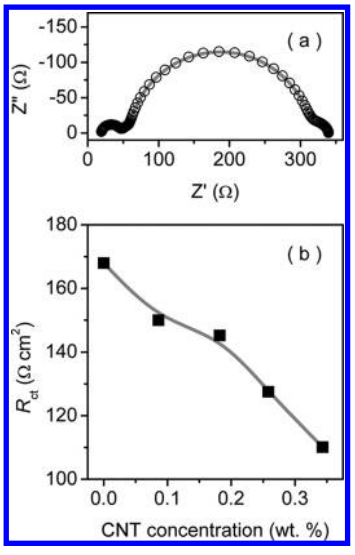

Figure 8. (a) Typical impedance spectrum for dye-sensitized solar cells. (b) Comparison for the interfacial charge transfer resistance of the cell with various concentrations of carbon nanotubes in the semiconductor electrodes.

dx.doi.org/10.1021/jp304845t | J. Phys. Chem. C 2012, 116, 14848−14856

cell can be obtained by fitting the EIS patterns using the transmission line model developed by Bisquert et al. (Figure 2a).[36−39] Figure 8b shows the R_{ct} value for each cell with various CNT concentrations in the semiconductor electrodes. It can be seen that the R_{ct} values monotonously decrease in the plot, suggesting that charge recombination becomes severe with CNT concentration increasing.

Since the photocurrent densities of the photovoltaic devices do not monotonously increase with the CNT concentration, the intrinsic feature of the carbon nanostructures should be taken into account. As it is well known that carbon species, including carbon black, activated carbon, graphene, as well as CNTs, possesses catalytic activities for conversion of iodine species. In addition, application of carbon materials as catalyst in the counter electrode of DSSCs for catalytic conversion of triiodide to iodide ions has been reported elsewhere,[23,52−58] while in the semiconductor electrode side conversion of triiodide to iodide ions means loss (recombination) of the photogenerated electrons, which is unfavorable to charge collection and should be suppressed. Thus, introduction of these materials into the semiconductor electrode would result in undesirable aggravation of charge recombination, since the carbon species (CNTs) in the composite cannot to be totally covered by the TiO_2 and direct exposure of the naked CNTs to the electrolyte is unavoidable (Figure 9). The extra reaction of

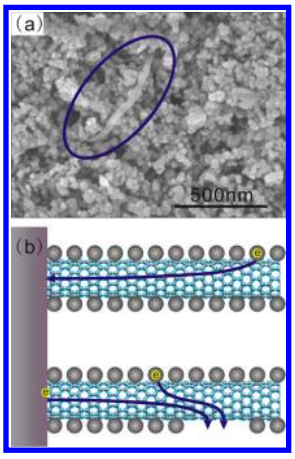

Figure 9. (a) Naked carbon nanotube observed on the surface of the semiconductor electrode. (b) Schematic diagram for leakage of photogenerated electrons from the semiconductor electrode to the electron acceptors in the electrolyte via the naked part of the carbon nanotube.

photogenerated electrons with the triiodide ions on the electrode−electrolyte interface via the naked CNTs will aggravate charge recombination in the whole voltage range during operation of the cells.

Having investigated the phenomena of the effect of CNTs on the transport properties of charge in the electrode and charge collection of the cell, the influence on the related electronic process and the photovoltaic characteristics will be examined in the following section.

3.3. Metal−Semiconductor Contact and Schottky Barrier. *3.3.1. General Description of Metal−Semiconductor Contact in DSSCs.* Generally, when a semiconductor contacts with metal, the Fermi level will become a constant through the system in thermal equilibrium. The type of the formed junction is commonly known as the Schottky barrier diode. Take the n-type semiconductor as an example, the electrons from the semiconductor will flow into the lower energy states in the metal side through the interface, the ideal energy band diagram for the isolated metal and semiconductor will change accordingly. Thus, the positively charged donor atoms remain in the semiconductor, creating a space charge region. As shown in Figure 10, the band in the semiconductor side in the formed

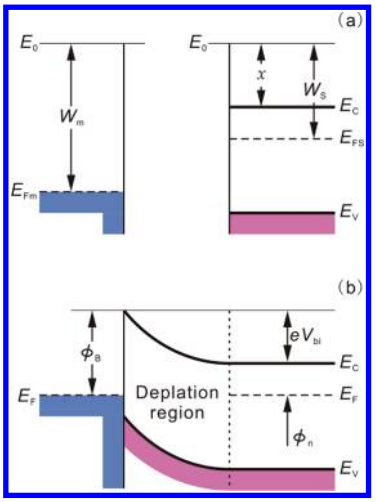

Figure 10. Energy band diagrams for isolated metal and semiconductor (a) and the formed Schottky barrier diode (b).

Schottky junction is upward bent. The Schottky barrier height, ϕ_B, of the metal−semiconductor contact can be given by

$$\phi_B = W_m - \chi \tag{4}$$

where W_m is work function of the metal and χ is the electron affinity of the semiconductor. On the semiconductor side, the built-in potential barrier, eV_{bi}, is be given by

$$eV_{bi} = W_m - \phi_n \tag{5}$$

where φ_n is the difference between the energy level of the low edge of the conduction band and the Fermi level of the semiconductor. In DSSCs, the materials used in the photoelectrode are low-doped n-type semiconductors, such as TiO_2 and ZnO. The basic electronic process during operation of the cells (under illumination) or under forward bias of the Schottky diode is transfer of photogenerated electrons over the potential barrier to the metal (or metal-like) substrate, which can be described by the thermionic emission theory. Thus, the flow of the electrons strongly depends on the height of the potential barrier, $e(V_{bi} - V_D)$. The net current density pass through the junction can be described as

$$J = \left(AT^2 \exp\left[\frac{-e\phi_B}{k_B T}\right]\right)\cdot\left(\exp\left[\frac{eV_D}{k_B T}\right] - 1\right) \tag{6}$$

in which A is the effective Richardson constant of the semiconductor for thermionic emission, V_D is the difference of the Fermi level between the metal and the semiconductor, k_B is the Boltzmann constant, and T is the temperature.

3.3.2. Improvement in Charge Collection by Reducing Grain Boundaries. For the common DSSCs (without CNTs in the semiconductor electrodes), the height of the Schottky contact barrier for the TCO−TiO_2 interface is only 0.2 eV (by adopting 4.4 eV for the work function of the FTO substrate and 4.2 eV for the conduction band level for the TiO_2 semi-

dx.doi.org/10.1021/jp304845t | J. Phys. Chem. C 2012, 116, 14848−14856

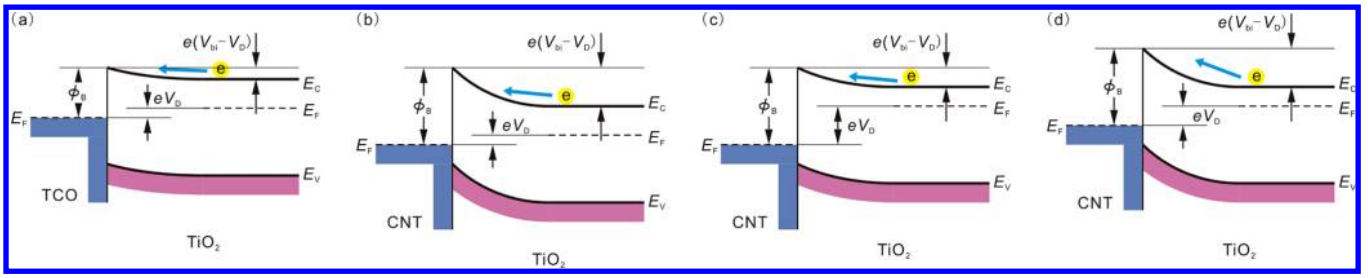

Figure 11. Energy band diagrams for the Schottky diodes of DSSCs under various conditions (not for scale). Comparison of the band diagrams for TCO−TiO_2 (a) and CNT−TiO_2 (b) junctions under identical illumination. Comparison of the band diagrams for CNTs-incorporated TiO_2 electrode under low (b) and high (c) illumination at short-circuit condition. Comparison of the band diagrams for the cell under identical illumination with low (c) and high (d) bias voltages. Note that the Fermi levels for the metal in a is higher than that in b and for the metal in d is upward shifted with respect to that in c.

conductor). While for the case of CNTs-incorporated TiO_2 electrode, ϕ_B has a value as high as 0.75 eV by adopting 4.95 eV as the work function for multiwalled carbon nanotubes.[59] When the cells are illuminated under identical light (the value of φ_n for each cell is identical as well), the height of the semiconductor-to-metal potential barrier, eV_{bi}, for the CNTs-incorporated electrode is much larger than that of the blank one. Thus, transfer of electrons from the TiO_2 to CNTs is energetically unfavorable, as compared with the case of the TCO−TiO_2 junction (Figure 11a and 11b). According to eq 6, the net current density (or the flow of electrons) in the Schottky junction was low for the CNTs-incorporated TiO_2 electrode, even in the case of the short-circuit condition, which is opposite to the photocurrent enhancement (Figures 5, 6, and 7b).

For the blank electrode, the collected photogenerated electrons would first undergo an encounter of a large number of interparticle boundaries and competing with recombination during the transport procedure before they transfer to the TCO substrate. Thus, the charge collection efficiency strongly depends on the thickness of the porous semiconductor film and the number of the grain boundaries encountered by the photogenerated electrons. For the case of CNTs-incorporated electrode, since the special *charge transport channels*, CNTs, are uniformly dispersed and embedded into the TiO_2 host, the required transport length for the collected photogenerated electrons to pass through the semiconductor film is much shorter. For example, for the blank TiO_2 electrode with a thickness of 10 μm (corresponding to a d = 1000 particle radii thick simulated film containing 10 nm radius particles), the average number of grain boundaries for the photogenerated electrons passing through the porous films is estimated to be $\sim 10^6$,[60] while for the CNTs-incorporated electrodes (0.1 wt %) the value for d is as low as ~35 particle radii thick (for a film with the same thickness of 10 μm), and the average number of grain boundaries should be much lower for electrons accessing the CNTs. The extremely low number of interparticle boundaries for electrons passing through the porous electrode will effectively save the charge from the trapping/detrapping-induced recombination on the grain boundaries, hence improving charge collection.

3.3.3. Transport of Photogenerated Electrons over the Potential Barrier. As mentioned above, although the height of the potential barrier, $e(V_{bi} - V_D)$, has an influence on the junction current, it would be not large when the density of electrons in the semiconductor is high (i.e., the value of φ_n is small, achieved by illumining the cells under relatively intense light) and the bias voltage of the cells is low. Under intense illumination, the electronic Fermi level of the semiconductor will shift toward higher energy level, resulting from injection of the photogenerated electrons. Thus, band bending (the height of the potential barrier) becomes lower (comparing Figure 11b and 11c) and transfer of charge from the semiconductor to the metal will take place. Thus, for the case of CNTs-incorporated TiO_2 electrode, in which the special charge channels are embedded into the host matrix, transport of electrons will be more efficient when we take the electrode as a whole (see Figure 4 and the high illumination intensity range of Figure 12).

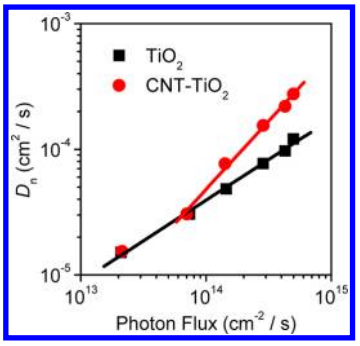

Figure 12. Diffusion coefficients of the photogenerated electrons in the semiconductor electrodes of the cells under various intensities of illumination.

When the illumination intensity is weak, the density of photogenerated electrons in the electrode is low. In this situation the Fermi level of the semiconductor becomes lower and band bending becomes larger (comparing Figure 11b and 11c). Therefore, transfer of electrons from the semiconductor side to the CNTs will be difficult. As the illumination is continuously lowered, CNTs will lose the role as the charge transport channels in the matrix, and transport of electrons in the electrode will rely on the host TiO_2 (Figure 12).

The photovoltaic characteristics strongly depend on the relationship between the charge transport behavior and the bias voltage of the cell. Since we investigated the effect of the illumination intensity on electron diffusion at short-circuit condition, the electron diffusion coefficients at various bias voltages for the cell will be explored. Upon constant illumination, an increase in the output voltage of the cell means variation of the electrode potential toward a more negative value (higher energy level). The situation is very similar to reducing the forward bias or extremely reverse bias to the Schottky junction (comparing Figure 11c and 11d). Thus,

dx.doi.org/10.1021/jp304845t | J. Phys. Chem. C 2012, 116, 14848−14856

during operation of the cells an increase in the output voltage will enlarge the height of the potential barrier.

Figure 13 presents the relationship for the change of the electron diffusion coefficients at various bias voltages obtained

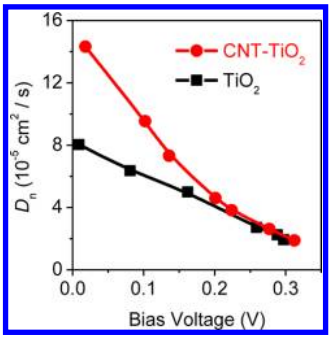

Figure 13. Diffusion coefficients of the photogenerated electrons in the semiconductor electrodes of the cells under various bias voltages. Biases of the cells have been corrected by iR_s drop.

under constant illumination of the cells. As it shows, the electron diffusion coefficients decrease as the bias voltage increases. In the low-bias voltage range the diffusion coefficient for the photogenerated electrons in the CNTs-incorporated electrode is nearly twice as large as that of the blank one. As the output voltage increases, the decrease in the electron diffusion coefficient for the CNTs-incorporated TiO_2 electrode is much more rapid, as compared with that of the blank one. When the voltage exceeds 0.2 V under illumination with an intensity of 2 mW/cm^2, the difference between the two electrodes is very tiny, suggesting CNTs lose their role as charge transport channels. In this situation the electrons will transport toward the TCO substrate though the mesoporous semiconductor network, rather than via the CNTs.

3.3.4. Combined Action of CNTs and TiO_2 for Energy Saving. The junction formed between the charge collector and the semiconductor, including the cases of the TCO−TiO_2 and CNT−TiO_2 junctions, will cause a loss of voltage and charge carriers (electrons) during operation of the cells. The power loss at the junction can be expressed as

$$P_{\text{loss}} = J \cdot \frac{k_B T}{e} \ln\left(1 + \frac{J}{AT^2 \exp[-e\phi_B/k_B T]}\right) \quad (7)$$

Clearly, the power loss increases with the height of the Schottky barrier, ϕ_B. According to the literature calculation,[61] energy dissipation on the junction is small when the height of the Schottky barrier is less than 0.5 eV. For common DSSCs, the height of the contact barrier on the TCO−TiO_2 interface is only 0.2 eV, which is very small and has almost no significant influence (power loss) on the output power of the cells.[61] When the value for the height of the contact barrier exceeds 0.6 eV, the energy dissipation on the junction will severely depress the output power of the devices.

Figure 14 presents the simulated $J-V$ plots for the cell with and without CNTs in the semiconductor electrodes.[62] As it shows, the cell with CNTs-incorporated electrodes exhibits relatively high values of photocurrent in the low-voltage range, while it decreases rapidly when the voltage is higher than 0.2 V, resulting in a very low value of *FF* as compared with that of the cell with a blank electrode. Thus, on the condition that transfer of the electrons to the TCO substrate was mediated via the

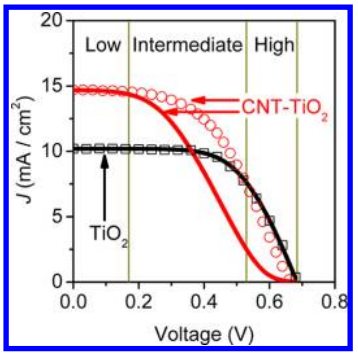

Figure 14. Experimental (black square and red cycle) and simulated (line) $J-V$ plots for the cells with blank and CNTs-incorporated TiO_2 semiconductor electrodes. Plane was divided into three voltage regions by the dark yellow lines according to the feature of the $J-V$ behavior. Detailed parameters adopted for the simulation: ideality factor, $m = 2$, series resistance, $R_s = 12\ \Omega$, saturation current, $J_0 = 1.7 \times 10^{-5}$ mA/cm^2, and short-circuit photocurrent densities were referred the experimental data.

CNTs over the whole voltage range, the energy conversion efficiency calculated from the simulated plots is only 3.71% for the CNTs-containing cells, which is lower than that of 4.34% for the blank cell, suggesting energy dissipation on the CNT−TiO_2 junction is very large. By comparing the simulated plots with the experimental data, it can be seen that both of them can match well with each other for the cell with a blank TiO_2 electrode. While for the case of the cell with CNT-incorporated electrode, the $J-V$ behavior of the simulated plots are rather different than the experimental data, especially in the relatively high-voltage region.

According to the experimental and simulated behavior and comparing them for cells with a blank and CNTs-incorporated electrodes, the plane in the $J-V$ plots should be divided into three regions: the low-voltage range, the intermediate-voltage range, and the high-voltage range (Figure 14). In the low-voltage range, the simulated and experimental $J-V$ behavior for the cell match well with each other, suggesting CNTs in the electrode can facilitate charge transport toward the TCO substrate. In this range, the CNTs undertake the role of special charge transport channels in the cell.

As the voltage increases, in the intermediate range, experimental data are starting to offset the simulated plots. While the photocurrent for the cell is still large, as compared with the $J-V$ curve for the blank one, even in the case the simulated current for the CNT-incorporated cell is lower. In this range, energy loss in the CNT−TiO_2 junctions becomes large and many of the CNTs are beginning to lose the role as charge transport channels. In this situation, electrons with relatively high energy would be able to overcome a potential barrier and transfer to the CNT charge collectors; the rest, however, whose energy is low, will diffuse through the porous TiO_2 network toward the TCO substrate. Thus, by virtue of the combination of CNTs and porous TiO_2 electrode for the transport of electrons, the collection efficiency for the photogenerated electrons is high and the number of them saved from recombination is relatively large, as compared with that of the blank cell.

As the voltage is continuously increasing, CNTs in the electrode will no longer aid the transport of electrons. Finally, the worse is CNTs totally lose their role of charge transport channels and only the opposite aspect remains. Leakage of the

dx.doi.org/10.1021/jp304845t | J. Phys. Chem. C 2012, 116, 14848−14856

electrons via the naked CNTs, which always take place during operation of the cell, will become a predominant feature of CNTs in the high-voltage range.

4. CONCLUSIONS

CNTs can promote transport of electrons in the semiconductor electrode of DSSCs, when the height of the semiconductor-to-metal potential barrier is not large. Under constant illumination, the CNTs gradually lose their role of charge transport channels and become totally charge leakage media as the output voltage increases. Thus, the $J-V$ behavior of the cells as well as the role of the CNTs can be divided into three stages. In the low-voltage range, the embedded CNTs can act as charge transport channels in the electrodes. Transport of the photogenerated electrons in the TiO_2 semiconductor particles injected from the excited dye molecules toward the TCO substrate will mediate by the CNTs, which will improve the charge transport performance and increase the charge collection efficiency. In the intermediate-voltage range, for charge collected by the TCO substrate, the contribution coming from the CNTs-mediated process becomes small as the voltage increases. In addition, the photocurrent of the cell decreases rapidly, due to the relatively large height of the potential barrier. At the high-voltage range, however, the role of CNTs is totally negative, charge leakage via the CNTs becomes predominant.

Further improvement in the photovoltaic performance of the DSSCs by incorporation of heterogeneous conducting nanostructures into the semiconductor can be achieved by modulating the energy band (to match well with the host semiconductor) to minimize power loss in the guest−host junction and the charge leakage via the guest materials should also be minimized by passivation of their ability to catalytic conversion of iodine species. We believe that our study on transport of charge in a CNT−TiO_2 composite electrode will help us to better understand the working principle of the cell. These findings here may provide important hints and will open up a way to further improve the photovoltaic performance of DSSCs.

■ ASSOCIATED CONTENT

Supporting Information

Infrared spectra of carbon nanotubes. This material is available free of charge via the Internet at http://pubs.acs.org.

■ AUTHOR INFORMATION

Corresponding Author

*E-mail: chenjiazang@hotmail.com (J.C.); zpzhu@sxicc.ac.cn (Z.Z.).

Present Address

†State Key Laboratory of High Performance Ceramics and Superfine Microstructure, Shanghai Institute of Ceramics, Chinese Academy of Sciences, Shanghai 200050, China.

Notes

The authors declare no competing financial interest.

■ ACKNOWLEDGMENTS

J.C. thanks Dr. Yinghua Xu (Zhejiang University of Technology) and Dr. Tiancheng Xu (HzCell Electrochem. Corp.) for help on the discussion of the charge transport project.

■ REFERENCES

(1) Oregan, B.; Gratzel, M. *Nature* **1991**, *353*, 737−740.
(2) Gratzel, M. *Nature* **2001**, *414*, 338−344.
(3) Yella, A.; Lee, H.-W.; Tsao, H. N.; Yi, C.; Chandiran, A. K.; Nazeeruddin, M. K.; Diau, E. W.-G.; Yeh, C.-Y.; Zakeeruddin, S. M.; Grätzel, M. *Science* **2011**, *334*, 629−634.
(4) Hagfeldt, A.; Gratzel, M. *Acc. Chem. Res.* **2000**, *33*, 269−277.
(5) Schlichthorl, G.; Park, N. G.; Frank, A. J. *J. Phys. Chem. B* **1999**, *103*, 782−791.
(6) Schlichthorl, G.; Park, N. G.; Frank, A. J. *Z. Phys. Chem, Int. J. Res. Phys. Chem. Chem. Phys.* **1999**, *212*, 45−50.
(7) Frank, A. J.; Kopidakis, N.; van de Lagemaat, J. *Coord. Chem. Rev.* **2004**, *248*, 1165−1179.
(8) Gratzel, M. *Inorg. Chem.* **2005**, *44*, 6841−6851.
(9) Ohsaki, Y.; Masaki, N.; Kitamura, T.; Wada, Y.; Okamoto, T.; Sekino, T.; Niihara, K.; Yanagida, S. *Phys. Chem. Chem. Phys.* **2005**, *7*, 4157−4163.
(10) Tan, B.; Wu, Y. Y. *J. Phys. Chem. B* **2006**, *110*, 15932−15938.
(11) Chen, J.; Li, B.; Zheng, J.; Jia, S.; Zhao, J.; Jing, H.; Zhu, Z. *J. Phys. Chem. C* **2011**, 7104−7113.
(12) Archana, P. S.; Jose, R.; Vijila, C.; Ramakrishna, S. *J. Phys. Chem. C* **2009**, *113*, 21538−21542.
(13) Wang, Q.; Zhang, Z.; Zakeeruddin, S. M.; Gratzel, M. *J. Phys. Chem. C* **2008**, *112*, 7084−7092.
(14) Chandiran, A. K.; Sauvage, F.; Casas-Cabanas, M.; Comte, P.; Zakeeruddin, S. M.; Graetzel, M. *J. Phys. Chem. C* **2010**, *114*, 15849−15856.
(15) Lu, X. J.; Mou, X. L.; Wu, J. J.; Zhang, D. W.; Zhang, L. L.; Huang, F. Q.; Xu, F. F.; Huang, S. M. *Adv. Funct. Mater.* **2010**, *20*, 509−515.
(16) Jang, S. R.; Vittal, R.; Kim, K. J. *Langmuir* **2004**, *20*, 9807−9810.
(17) Kongkanand, A.; Martinez Dominguez, R.; Kamat, P. V. *Nano Lett.* **2007**, *7*, 676−680.
(18) Ng, Y. H.; Lightcap, I. V.; Goodwin, K.; Matsumura, M.; Kamat, P. V. *J. Phys. Chem. Lett.* **2010**, *1*, 2222−2227.
(19) Kamat, P. V. *J. Phys. Chem. Lett.* **2011**, *2*, 242−251.
(20) Kim, S. L.; Jang, S. R.; Vittal, R.; Lee, J.; Kim, K. J. *J. Appl. Electrochem.* **2006**, *36*, 1433−1439.
(21) Zhang, S.; Niu, H.; Lan, Y.; Cheng, C.; Xu, J.; Wang, X. *J. Phys. Chem. C* **2011**, 22025−22034.
(22) Chan, Y.-F.; Wang, C.-C.; Chen, B.-H.; Chen, C.-Y. *Carbon* **2011**, *49*, 4898−4910.
(23) Chen, T.; Qiu, L.; Cai, Z.; Gong, F.; Yang, Z.; Wang, Z.; Peng, H. *Nano Lett.* **2012**, *12*, 2568−2572.
(24) Tang, Y. B.; Lee, C. S.; Xu, J.; Liu, Z. T.; Chen, Z. H.; He, Z. B.; Cao, Y. L.; Yuan, G. D.; Song, H. S.; Chen, L. M.; Luo, L. B.; Cheng, H. M.; Zhang, W. J.; Bello, I.; Lee, S. T. *ACS Nano* **2010**, *4*, 3482−3488.
(25) Yang, N. L.; Zhai, J.; Wang, D.; Chen, Y. S.; Jiang, L. *ACS Nano* **2010**, *4*, 887−894.
(26) Kamat, P. V.; Tvrdy, K.; Baker, D. R.; Radich, J. G. *Chem. Rev.* **2010**, *110*, 6664−6688.
(27) Manga, K. K.; Zhou, Y.; Yan, Y. L.; Loh, K. P. *Adv. Funct. Mater.* **2009**, *19*, 3638−3643.
(28) Yen, M.-Y.; Hsiao, M.-C.; Liao, S.-H.; Liu, P.-I.; Tsai, H.-M.; Ma, C.-C. M.; Pu, N.-W.; Ger, M.-D. *Carbon* **2011**, *49*, 3597−3606.
(29) Hayashi, H.; Lightcap, I. V.; Tsujimoto, M.; Takano, M.; Umeyama, T.; Kamat, P. V.; Imahori, H. *J. Am. Chem. Soc.* **2011**, *133*, 7684−7687.
(30) Guo, W.; Xu, C.; Wang, X.; Wang, S.; Pan, C.; Lin, C.; Wang, Z. L. *J. Am. Chem. Soc.* **2012**, *134*, 4437−4441.
(31) Fang, X.; Li, M.; Guo, K.; Zhu, Y.; Hu, Z.; Liu, X.; Chen, B.; Zhao, X. *Electrochim. Acta* **2012**, *65*, 174−178.
(32) Kim, D. Y.; Kim, J.; Kim, J.; Kim, A. Y.; Lee, G.; Kang, M. *J. Ind. Eng. Chem.* **2012**, *18*, 1−5.
(33) Kyaw, A. K. K.; Tantang, H.; Wu, T.; Ke, L.; Wei, J.; Demir, H. V.; Zhang, Q.; Sun, X. W. *J. Phys. D: Appl. Phys.* **2012**, *45*, 165103.

(34) Dang, X.; Yi, H.; Ham, M.-H.; Qi, J.; Yun, D. S.; Ladewski, R.; Strano, M. S.; Hammond, P. T.; Belcher, A. M. *Nat Nano* **2011**, *6*, 377−384.
(35) Wang, S.; Yi, L.; Halpert, J. E.; Lai, X.; Liu, Y.; Cao, H.; Yu, R.; Wang, D.; Li, Y. *Small* **2012**, *8*, 265−271.
(36) Bisquert, J. *J. Phys. Chem. B* **2001**, *106*, 325−333.
(37) Fabregat-Santiago, F.; Garcia-Belmonte, G.; Bisquert, J.; Zaban, A.; Salvador, P. *J. Phys. Chem. B* **2002**, *106*, 334−339.
(38) Fabregat-Santiago, F.; Bisquert, J.; Garcia-Belmonte, G.; Boschloo, G.; Hagfeldt, A. *Sol. Energy Mater. Sol. Cells* **2005**, *87*, 117−131.
(39) Fabregat-Santiago, F.; Bisquert, J.; Palomares, E.; Otero, L.; Kuang, D. B.; Zakeeruddin, S. M.; Gratzel, M. *J. Phys. Chem. C* **2007**, *111*, 6550−6560.
(40) Yen, C. Y.; Lin, Y. F.; Liao, S. H.; Weng, C. C.; Huang, C. C.; Hsiao, Y. H.; Ma, C. C. M.; Chang, M. C.; Shao, H.; Tsai, M. C.; Hsieh, C. K.; Tsai, C. H.; Weng, F. B. *Nanotechnology* **2008**, *19*, 375305.
(41) Chen, J.; Li, B.; Zheng, J.; Zhao, J.; Jing, H.; Zhu, Z. *Electrochim. Acta* **2011**, *56*, 4624−4630.
(42) Kavan, L.; Bacsa, R.; Tunckol, M.; Serp, P.; Zakeeruddin, S. M.; Le Formal, F.; Zukalova, M.; Graetzel, M. *J. Power Sources* **2010**, *195*, 5360−5369.
(43) Bisquert, J. *Phys. Chem. Chem. Phys.* **2008**, *10*, 49−72.
(44) Tiedje, T.; Cebulka, J. M.; Morel, D. L.; Abeles, B. *Phys. Rev. Lett.* **1981**, *46*, 1425−1428.
(45) Orenstein, J.; Kastner, M. *Phys. Rev. Lett.* **1981**, *46*, 1421−1424.
(46) van de Lagemaat, J.; Frank, A. J. *J. Phys. Chem. B* **2001**, *105*, 11194−11205.
(47) Dloczik, L.; Ileperuma, O.; Lauermann, I.; Peter, L. M.; Ponomarev, E. A.; Redmond, G.; Shaw, N. J.; Uhlendorf, I. *J. Phys. Chem. B* **1997**, *101*, 10281−10289.
(48) Kruger, J.; Plass, R.; Gratzel, M.; Cameron, P. J.; Peter, L. M. *J. Phys. Chem. B* **2003**, *107*, 7536−7539.
(49) Quaranta, S.; Gozzi, D.; Tucci, M.; Lazzarini, L.; Latini, A. *J. Power Sources* **2012**, *204*, 249−256.
(50) Sun, S. R.; Gao, L. A.; Liu, Y. Q. *Thin Solid Films* **2011**, *519*, 2273−2279.
(51) Zaban, A.; Greenshtein, M.; Bisquert, J. *ChemPhysChem* **2003**, *4*, 859−864.
(52) Kay, A.; Gratzel, M. *Sol. Energy Mater. Sol. Cells* **1996**, *44*, 99−117.
(53) Lee, W. J.; Ramasamy, E.; Lee, D. Y.; Song, J. S. *ACS Appl. Mater. Interfaces* **2009**, *1*, 1145−1149.
(54) Kitamura, T.; Maitani, M.; Matsuda, M.; Wada, Y.; Yanagida, S. *Chem. Lett.* **2001**, 1054−1055.
(55) Jia, R.; Chen, J.; Zhao, J.; Zheng, J.; Song, C.; Li, L.; Zhu, Z. *J. Mater. Chem.* **2010**, *20*, 10829−10834.
(56) Kavan, L.; Yum, J. H.; Grätzel, M. *ACS Nano* **2011**, *5*, 165−172.
(57) Kavan, L.; Yum, J.-H.; Nazeeruddin, M. K.; Grätzel, M. *ACS Nano* **2011**, *5*, 9171−9178.
(58) Kavan, L.; Yum, J.-H.; Grätzel, M. *Nano Lett.* **2011**, *11*, 5501−5506.
(59) Shiraishi, M.; Ata, M. *Carbon* **2001**, *39*, 1913−1917.
(60) Benkstein, K. D.; Kopidakis, N.; van de Lagemaat, J.; Frank, A. J. *J. Phys. Chem. B* **2003**, *107*, 7759−7767.
(61) Ni, M.; Leung, M. K. H.; Leung, D. Y. C.; Sumathy, K. *Sol. Energy Mater. Sol. Cells* **2006**, *90*, 2000−2009.
(62) Soedergren, S.; Hagfeldt, A.; Olsson, J.; Lindquist, S.-E. *J. Phys. Chem.* **1994**, *98*, 5552−5556.